Damaging Graphene with Ozone Treatment: A Chemically Tunable Metal−Insulator Transition

Nicolas Leconte,[†] Joël Moser,[‡] Pablo Ordejón,[‡] Haihua Tao,[‡] Aurélien Lherbier,[†] Adrian Bachtold,[‡] Francesc Alsina,[‡] Clivia M. Sotomayor Torres,[‡,§] Jean-Christophe Charlier,[‡] and Stephan Roche[§,⊥,*]

[†]IMCN, Université Catholique de Louvain, Place Croix du Sud 1 (PCPM-ETSF), B-1348 Louvain-la-Neuve, Belgium, [‡]CIN2 (ICN-CSIC) Barcelona, Campus UAB, E08193 Bellaterra, Spain, [§]ICREA, 08010 Barcelona, Spain, and [⊥]CEA, INAC, SP2M, L_Sim, 17 avenue des Martyrs, 38054 Grenoble, France

ABSTRACT We present a multiscale *ab initio* study of electronic and transport properties of two-dimensional graphene after epoxide functionalization *via* ozone treatment. The orbital rehybridization induced by the epoxide groups triggers a strong intervalley scattering and changes dramatically the conduction properties of graphene. By varying the coverage density of epoxide defects from 0.1 to 4%, charge conduction can be tuned from a diffusive to a strongly localized regime, with localization lengths down to a few nanometers long. Experimental results supporting the interpretation as a metal−insulator transition are also provided.

KEYWORDS: disordered graphene · quantum transport · metal−insulator transition · ozone treatment · numerical simulation

The discovery of graphene in early 2004[1,2] has sparked intense theoretical and experimental activities, opening new prospects in carbon-based nanoelectronics.[3,4] Indeed, pristine graphene exhibits genuinely large charge mobilities, and in the low density limit (close to the Dirac point), the measured conductivities are weakly temperature-dependent ranging typically within 2−15 e^2/h. Conduction in a clean graphene monolayer deposited on an oxide substrate is limited by long-range scattering induced by charges trapped in the oxide, by mechanical deformations (ripples), or by weakly bonded adsorbed impurities.[5,6] At low temperatures, weak localization and weak antilocalization regimes have been theoretically discussed[7,8] and experimentally reported,[9] but to date, no insulating state could be observed in clean graphene.

The tuning of graphene electronic properties by chemical functionalization has opened a new era of solid-state electronics and of composite materials. Indeed, chemical functionalization of graphene can be a way to enhance the functionalities or improve the performance of graphene-based devices.[10−16] The severe modification of sp^2-bonded carbon materials by ion irradiation[17] or intentional introduction of sp^3 defects also suggests a route to produce strong enough disorder in graphene to observe localization phenomena.[18−22] In the situation of a nearly complete oxidation of the graphene sheet, the material becomes a sp^3 chemical derivative of graphene,[23−25] with sheet resistance several orders of magnitude higher than clean graphene, reaching the MΩ or GΩ regimes[26] (for a recent review, see ref 27). Additionally, a strongly invasive hydrogenation treatment of suspended graphene can turn the material into *graphane*, a true band insulator.[28]

Several possibilities to tune in a smooth fashion the conduction of graphene from the semimetallic to the insulating state by means of either ion irradiation[29] and partial hydrogenation[30] have been recently explored. In the latter experiment, the band structure (followed by ARPES measurements) was found to remain gapless upon a moderate increase of hydrogen coverage, whereas a significant drop of the conductance was assigned to the signature of the Anderson insulating state.[30] To date, the chemical functionalization conditions for a fine-tuning of the graphene damage and control of the resulting two-dimensional metal−insulator transition remain to be fully established.

In this article, the electronic and transport properties of ozone-treated graphene are investigated using *ab initio* calculations and a real space order-N transport computational methodology based on a reparametrized tight-binding Hamiltonian. Ozone molecules adsorb on the graphene basal plane with a binding energy of 0.25 eV, and the physisorbed molecules can chemically react with graphene to form epoxide groups and oxygen molecules.[31]

*Address correspondence to stephan.roche@cea.fr.

Received for review March 16, 2010 and accepted June 22, 2010.

Published online July 12, 2010.
10.1021/nn100537z

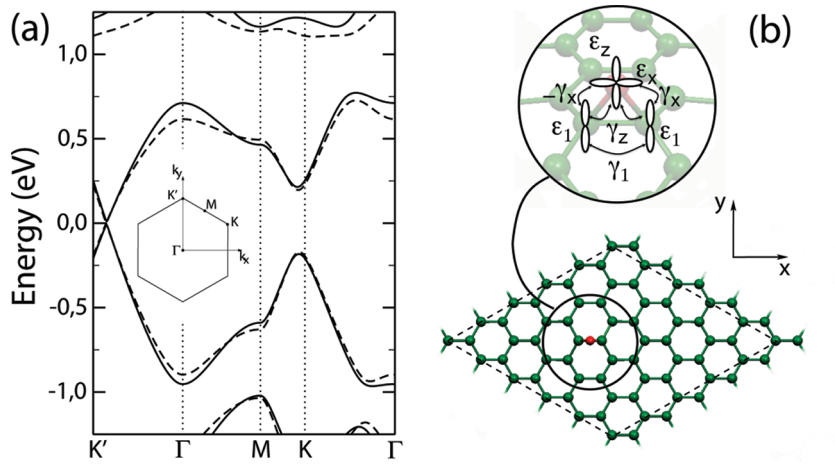

Figure 1. (a) DFT (dashed lines) and TB (solid lines) band structures of graphene decorated with a single epoxide group per 5 × 5 supercell (b). The labeling of the high symmetry points of the supercell Brillouin zone is shown in the inset (a). Scheme for the TB parameters in the epoxide group is also illustrated in (b).

The C−O bonding distance of the epoxide group has been found to be 1.44 Å,[31] pointing toward a sp^3 bonding, as also confirmed by the computed 3.23 eV desorption energy into an atomic oxygen. This makes the epoxide group very stable in the absence of reverse reaction. Given that physisorbed oxygen molecules are known to weakly impact the electronic properties of carbon-based materials, we focus on the effect of a varying density of epoxide groups grafted on the graphene basal plane and assume an homogeneous coverage and weak density. Our calculations evidence the continuous transition from a conductive to a strongly insulating behavior as the epoxide coverage reaches a few percent. The simulations are complemented with experimental measurements that confirm the tendency of such chemically functionalized material to exhibit an insulating regime.

RESULTS AND DISCUSSION

At first, a graphene monolayer with a single epoxide group repeated with a $\sqrt{3} \times \sqrt{3}$ periodicity (one oxygen atom per six carbon atoms) is numerically investigated. The DFT band structure (see Methods) is computed and used to extract a minimal tight-binding (TB) model able to describe the states near the Fermi energy and to provide a simplified TB Hamiltonian that will be used for transport calculations. For graphene, a standard π electron orthogonal TB model is assumed with first neighbor interactions parametrized using a conventional hopping integral $\gamma_0 = -2.6$ eV. To account for the effect of the epoxide group, p_x and p_z orbitals of the oxygen impurity (where z is the direction perpendicular to the graphene sheet, and x is the direction of the epoxide group) are found to be sufficient to provide an accurate fit of the DFT band structure around the Fermi level. The presence of oxygen also changes the diagonal energy of the carbon atoms to which it bonds, as well as their mutual interaction. The parameters extracted from the fit are $\varepsilon_x = -2.5$ eV, $\varepsilon_z = -1.0$ eV, $\varepsilon_1 = 1.5$ eV, $\gamma_x = 1.8\gamma_0$, $\gamma_z = -1.5\gamma_0$, and $\gamma_1 = 0.0$ (see Figure 1b for notation). Then, the quality of the TB parameter set is tested by comparison with the DFT band structure of a 5×5 graphene supercell containing a single epoxy group (Figure 1a), therefore having a significantly smaller concentration of impurities than the $\sqrt{3} \times \sqrt{3}$ model used for the fitting.

One notes that for the chosen epoxy conformation (Figure 1a), a K−K′ degeneracy lifting is provoked by symmetry breaking: unlike the clean case, a gap is found in the vicinity of the K-point, whereas a linear band crossing is observed close to the K′ point. A different orientation of the defect (not shown here) pro-

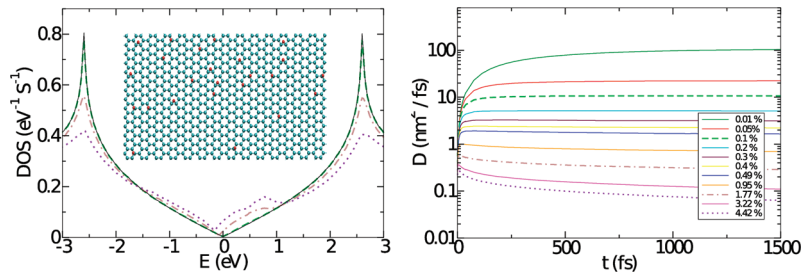

Figure 2. Left panel: Total density of states of pristine graphene (bold solid line) and chemically modified graphene with varying density of grafted epoxide groups (mainframe). Inset: Ball-and-stick model illustrates a disordered sample (red color is for oxygen atoms) with defect density of 3.2%. Right panel: Time-dependent evolution of the diffusion coefficient of quantum wavepackets at energy $E = 0.5$ (see text).

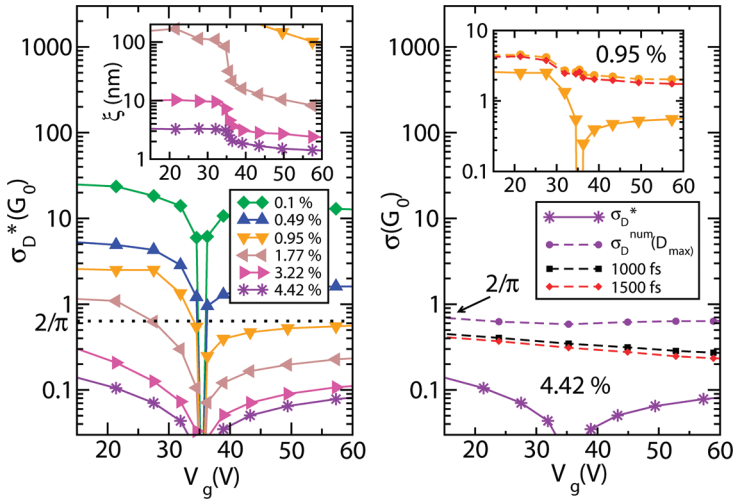

Figure 3. Left panel: $\sigma^*_D(V_g)$ (main frame) of chemically-modified graphene for several epoxide-defects densities n_i = 0.1−4.42%. Right panel: Kubo conductivities for n_i = 4.42% (main frame) and n_i = 0.95% (inset) at different elapsed computational times. $\sigma^*_D(V_g)$ at n_i = 4.42% is also given for comparison. The localization lengths computed using $\xi(E) = \ell_e \exp(\pi\sigma_D^{num}(E)/2G_0)$ are also given (left panel, inset).

duces a symmetric behavior. One also notes that the extracted tight-binding parameters for one case fully reproduce the *ab initio* results in the other case, which guarantees the validity of the parametrization. Additionally, since the rest of the study concerns large disordered systems, the consequences of symmetry breaking observed for small supercells are lifted and the studied system remains gapless.

Figure 2 displays the evolution of the total density of states (DoS) as a function of the epoxide group coverage (from n_i = 0.01 up to 4.42%) obtained with the TB model. Defect densities below ≃0.1% weakly affect the DoS, which remains similar to that of pristine graphene (bold solid lines). However, as the impurity density (n_i) is further increased, several noticeable features are observed. An accumulation of epoxide-induced quasi-bound states takes place close to the Dirac point and triggers the emergence of a broad peak on the donor side (in agreement with prior calculations[32,33]). This peak widens and increases with n_i, whereas the DoS at the Dirac point is also enhanced because of disorder. Such effects are also accompanied by a continuous decay and smoothing of the two van Hove singularities present at higher energies ($\pm\gamma_0$).

To explore the transport properties of disordered graphene, we use an efficient real space order-N method which allows one to simultaneously follow the wavepacket dynamics and compute the Kubo conductivity (see Methods). The evolution of the wavepacket dynamics at E = 0.5 eV for several epoxide group densities (n_i) is reported in Figure 2 (right panel). As long as $n_i \leq 0.5\%$, the diffusion coefficient is found to reach a saturation regime after a few thousand femtoseconds, and then remains almost constant up to very long times, indicating a diffusive regime (note that for n_i = 0.01%, saturation time is higher than 2000 fs) and a vanishingly small contribution of quantum interferences within the computational reach. The maximum value allows the evaluation of $l_e = D_{max}/v_F$, with $v_F = 10^6$ ms^{-1}.

Close to the Dirac point, an approximative Drude conductivity $\sigma^*_D(E)$ can be extracted from the computed elastic mean free path and the analytical DoS. Using $\rho(E) = 2|E|/(\pi \times (\hbar v_F)^2)$, the Drude formula reads $\sigma^*_D(E) = (4e^2/h) \times k l_e(E)/2$, with $E = \hbar v_F k$. Additionally, the energy scale can be converted into a gate voltage unit using $k = \sqrt{\pi n}$ (where n is the electronic density), so that $\sigma^*_{Drude} = 2e^2/h(\sqrt{\pi C_g V_g/e})l_e$ ($C_g \simeq 1.15 \times 10^{-4}$ Fm^{-2} is the estimated experimental gate capacitance).[34] A theoretical $\sigma^*_{Drude}(V_g)$ is thus obtained as a function of n_i (see Figure 3, left panel). One first observes a significant electron−hole asymmetry of $\sigma^*_{Drude}(V_g)$ for the considered epoxide coverages. Besides, $\sigma^*_{Drude}(V_g)$ is seen to downscale as $\simeq 1/n_i$ following a Fermi Golden Rule argument, and irrespective of the considered location of the Fermi energy, which is actually in sharp contrast with the case of substitutional (boron) impurities.[35] Indeed for boron substitutions (which preserve the sp^2 symmetry), the minimum Drude conductivity was found to always remain larger than $G_0 = 2e^2/h$ even for densities as large as 4%.[35] Here the approximation of a disorder-independent density of states yields $\sigma^*_D(E) \to 0$ close to the Dirac point, which is in contradiction with the semiclassical result ($4e^2/\pi h$) obtained within the Born approximation by Shon and Ando.[36]

To go beyond such approximation, the scaling analysis of the conductivity can be carried out using the Kubo formula $\sigma(E,t) = (e^2/2)\mathrm{Tr}[\delta(E - \hat{H})]D(E,t)$ where $\mathrm{Tr}[\delta(E - \hat{H})/S]$ is the DoS per unit of surface at Fermi energy E. At a fixed energy, $\sigma(E,t)$ reaches its maximal value at the same time as $D(E,t)$ (D_{max}), which provides an alternative estimation of the Drude conductivity

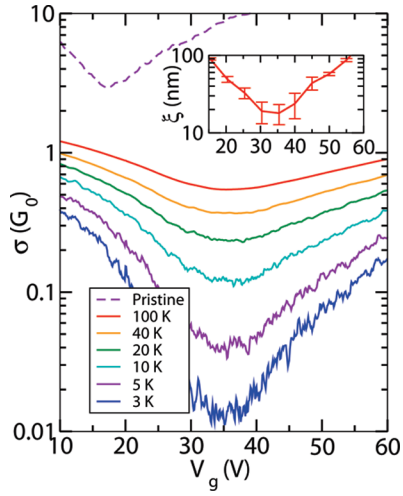

Figure 4. Four-terminal conductivity (mainframe) as a function of the applied gate voltage for a graphene sample exposed to ozone (see text). Data were taken at various temperatures T = 3, 5, 10, 20, 40, and 100 K (from bottom to top). The conductance curve at 5 K before ozone treatment is also shown as dashed lines for comparison. Inset: Gate-dependent localization length (red line with error bars) estimated from a variable range hopping behavior.

$(\sigma^{num}_{Drude}(E) = (e^2/2)\mathrm{Tr}[\delta(E - \hat{H})]D_{max}(E))$ that here accounts for the disorder effects on the density of states. Figure 3 (right panel, main frame) shows that the decay of $\sigma^{num}_{Drude}(E)$ for the largest density $n_i = 4.42\%$ saturates at $4e^2/\pi h = 2G_0/\pi$.

Furthermore, the increasing contribution of quantum interferences can be actually followed by the scaling analysis, using the elapsed time during wavepacket propagation as the scaling parameter. For instance, in Figure 2 (right panel), starting from $n_i \simeq 0.95\%$, the saturation regime of $D(t)$ is seen to be immediately followed by a marked decay of $D(t)$, which is a clear signature of the onset of localization phenomena. Increasing n_i progressively sharpens the diffusive regime and generates stronger localization effects at shorter times. In Figure 3 (right panel), the scaling behavior of the conductivity is further illustrated deep into the diffusive regime for two different propagation times (1000 and 1500 fs) and $n_i = 4.42\%$. As obtained for the diffusion coefficient, the contributions of quantum interferences accumulate with time and yield a time-dependent (or length-dependent) conductance decay (see Figure 3 (right panel)), which becomes stronger with increasing n_i. As predicted by the conventional scaling theory of localization, such quantum interferences will turn the material to an Anderson insulator.[37]

To confirm the impact of ozone functionalization on transport in graphene, experiments were performed. Graphene samples were prepared by exfoliation of Kish graphite on a substrate of silicon overgrown with 300 nm of thermal silicon oxide. Electrodes were then patterned in a four-terminal configuration by electron beam lithography and Cr/Au deposition. The silicon substrate acts as a backgate electrode that tunes the charge density within graphene. Fabrication residues were removed by placing the samples in a flow of Ar/H_2 at 300 °C for a few hours, ensuring that the graphene surface will uniformly react with ozone. Then, samples were placed in an ozone atmosphere produced by UV decomposition of oxygen gas for a few minutes. The defects produced on the sample were monitored by following the evolution of the corresponding typical D-mode signature in the Raman spectroscopy spectra (not shown here). Finally, the conductivities of the samples were measured using a high input impedance lock-in technique at various temperatures and as a function of applied gate voltage (Figure 4). The onset of strong localization is featured by the dramatic decay of the conductivity *versus* temperature, especially for $V_g \simeq 36$ V, which locates the position of the shifted Dirac point induced by p-doping. By applying a magnetic field, a continuous transition from a weak to a strong localization regime is unveiled.[38] Similar to the theoretical result, the gate dependence of the measured conductivity also shows a weak electron−hole asymmetry, with higher hole conductivity.

A quantitative comparison between the simulations and the experiments is a difficult task. First, a more precise experimental characterization of the ozone-modified graphene sample (to determine defects type, density, and distribution) would be desirable for a direct comparison, but the required complementary analysis (*i.e.*, STM) is beyond the scope of the present study. Additionally, the measured conductivity contains contributions of quantum interferences as well as inelastic scattering mechanisms which drive its absolute value as well as its temperature dependence. At a fixed temperature, the transport regime turns out to be dependent on the energy of charge carriers and can range from weak to strong localization.

In the weak localization regime, the decay of the experimental conductance with decreasing temperature is driven by the increase of the coherence length (L_φ) (or say differently by an enhancement of quantum interferences correction). Electron−phonon or electron−electron scatterings are the main microscopic mechanisms of decoherence driven by the temperature. In contrast, the simulations are performed at zero temperature, but as shown in Figure 3, the Kubo conductance retains all quantum interference effects and thus decreases for longer elapsed times for the wavepacket propagation. The scaling parameter of the simulated conductance is thus somewhat a different (but equivalent) way to tune the contribution of quantum interferences. However, to achieve a full quantitative comparison between theory and experiments, a microscopic (temperature-dependent) decoherence mechanism (such as electron−phonon or electron−electron scat-

tering) should be introduced in the simulation. This is a very complex issue, although it could be possible to account for effective electron−phonon scattering by combining the Kubo method with classical molecular dynamics, as recently proposed by Ishii and co-workers for studying decoherence effects in carbon nanotubes.[40]

One should also note that the coherence length (tuned by the temperature in the experiment) should be compared to the localization length computed at zero temperature (as discussed in ref 38). Actually, by analyzing the temperature dependence of the experimental conductivity in the very low temperature regime, some rough estimate of a localization length can be given and contrasted with the simulation. Following prior works on oxidized graphene,[23,24] the experimental data are fitted using the conventional variable range hopping law $\sigma(T) = \exp(-(T_0/T)^{1/3})$, from which $\xi = \sqrt{13.8/k_B\rho T_0}$ can be extracted, as illustrated in Figure 4 (inset). Furthermore, an approximate estimate of the theoretical localization lengths can be also achieved using the general relationship between main transport length scales $\xi = l_e\exp(\pi\sigma_{Drude}/2G_0)$.[37] The obtained $\xi(E)$ values are displayed in Figure 3 (left panel, inset) and range from several tens of nanometers down to a few nanometers depending on the gate voltage and epoxide density. The weak electron−hole asymmetry gate dependence observed for the measured conductivity is not obvious in the corresponding experimental ξ, but the comparison between experimental values and simulations, however, suggests that an epoxide density of a few percent could suffice to drive the system to the strong insulating regime.

CONCLUSIONS

To conclude, a first-principles study of electronic and quantum transport properties of disordered graphene covered with ozone-induced epoxide defects has been presented. A drastic decrease of conductivity is theoretically predicted as a function of epoxide density, leading to a strong insulating state for densities of epoxide defects of only a few percent. Surprisingly, a slight exposure to ozone (that is, a low ozone coverage) is shown to have a dramatic impact on the transport properties of graphene. Accordingly, our results open a route to tune the Anderson metal−insulator transition in chemically modified graphene. One finally notes that oxygen adatoms covalently bind to graphene, without introducing midgap states as both graphene sublattices are equally affected by the epoxy defect.[33] This is not the case for hydrogen adatoms or vacancies which can produce local magnetism (for a review, see ref 41).

METHODS

Density functional theory (DFT) calculations are used to study both the atomic structure and the electronic properties of epoxide groups in graphene. The DFT calculations are performed using the Siesta code,[42] within the local density approximation (LDA) to the exchange-correlation functional in the Ceperley−Alder[43] form, as parametrized by Perdew and Zunger.[44] Pseudopotentials of the Troullier−Martins type[45] are used to account for the effect of core electrons. At last, the wave functions of the valence electrons are expanded in a double-ζ polarized basis set of finite-range numerical pseudoatomic orbitals.[46]

To simulate transport properties of large and disordered graphene systems, an efficient order-N quantum wavepacket approach is employed.[35,47−50] In this formalism, the mean free path $l_e(E)$ and the semiclassical conductivity $\sigma_{Drude}(E)$ are deduced from the time dependence of the diffusion coefficient $D(E,t)$ which is derived from[49]

$$D(E,t) = \frac{1}{t}\frac{\sum_n \langle\Psi_n|\delta(E-\hat{H})(\hat{U}^\dagger(t)\hat{x}\hat{U}(t)-\hat{x})^2|\Psi_n\rangle}{\sum_m \langle\Psi_m|\delta(E-\hat{H})|\Psi_m\rangle}$$

where $\hat{x}$ is the position operator along the x (transport) direction, in the Schrödinger representation. To evaluate $D(t)$, the dynamics of electronic wave-packets $|\Psi_n\rangle$ are followed through the time-evolution operator $\hat{U}(t) = \prod_{n=0}^{N-1}\exp(i\hat{H}(n\Delta t)\Delta t/\hbar)$ with $\hat{H}(t)$ and Δt the chosen time step. Using a Chebyshev polynomial expansion method for $\hat{U}(t)$, an order-N calculation allows to achieve transport calculations in systems containing millions of carbon atoms.[49] Several initial electron wavepackets are used. The calculations are performed for $D(t)$ up to $t \approx 3800$ fs with $\Delta t \equiv 0.1 \times h/(1\text{ eV}) = 0.41$ fs for graphene systems several hundreds of nanometers squared, applying periodic boundary conditions. Such a technique has already been successfully applied to carbon nanotubes and graphene.[35]

Acknowledgment. J.-C.C. acknowledges financial support from the F.R.S.-FNRS of Belgium. Parts of this work are directly connected to the Belgian PAI-VI Program on "Quantum Effects in Clusters and Nanowires" and to the ARC "NANHYMO" sponsored by the Communauté Française de Belgique. This work was partly funded by the European Union under Contract No. 215752 "GRAND" and by the NANOSIM-GRAPHENE Project No. ANR-09-NANO-016-01 funded by the French National Agency (ANR) in the frame of its 2009 programme in Nanosciences, Nanotechnologies & Nanosystems (P3N2009). P.O. acknowledges support from Spanish MICINN Grant FIS2009-12721-C04-01.

REFERENCES AND NOTES

1. Novoselov, K. S.; Jiang, D.; Schedin, F.; Booth, T. J.; Khotkevich, V. V.; Morozov, S. V.; Geim, A. K. Two-Dimensional Atomic Crystals. *Proc. Natl. Acad. Sci. U.S.A.* **2005**, *102*, 10451–10453.
2. Castro Neto, A. H.; Guinea, F.; Peres, N. M. R.; Novoselov, K. S.; Geim, A. K. The Electronic Properties of Graphene. *Rev. Mod. Phys.* **2009**, *81*, 109.
3. Lemme, M. Current Status of Graphene Transistors. *Solid State Phenomena* **2010**, *499*, 156.
4. Yamaguchi, H.; Eda, G.; Mattevi, C.; Kim, H.; Chhowalla, M. Highly Uniform 300 mm Wafer-Scale Deposition of Single and Multilayered Chemically Derived Graphene Thin Films. *ACS Nano* **2010**, *4*, 524–528.
5. Tan, Y.-W.; Zhang, Y.; Bolotin, K.; Zhao, Y.; Adam, S.; Hwang, E. H.; Das Sarma, S.; Stormer, H. L.; Kim, Ph. Measurement of Scattering Rate and Minimum Conductivity in Graphene. *Phys. Rev. Lett.* **2007**, *99*, 246803.

6. Adam, S.; Hwang, E. H.; Galitski, V. M.; Das Sarma, S. A Self-Consistent Theory for Graphene Transport. *Proc. Natl. Acad. Sci. U.S.A.* **2007**, *104*, 18392.
7. Suzuura, H.; Ando, T. Crossover from Symplectic to Orthogonal Class in a Two-Dimensional Honeycomb Lattice. *Phys. Rev. Lett.* **2002**, *89*, 266603.
8. McCann, E.; Kechedzhi, K.; Fal'ko, V. I.; Suzuura, S.; Ando, T.; Altshuler, B. I. Weak-Localization Magnetoresistance and Valley Symmetry in Graphene. *Phys. Rev. Lett.* **2006**, *97*, 146805.
9. Tikhonenko, F. V.; Horsell, D. W.; Gorbachev, R. V.; Savchenko, A. K. Weak Localization in Graphene Flakes. *Phys. Rev. Lett.* **2008**, *100*, 056802.
10. Loh, K. P.; Bao, Q.; Ang, P. K.; Yang, J. The Chemistry of Graphene. *J. Mater. Chem.* **2010**, *20*, 2277–2289.
11. Schedin, F.; Geim, A. K.; Morozov, S. V.; Hill, E. W.; Blake, P.; Katsnelson, M. I.; Novoselov, K. S. Detection of Individual Gas Molecules Adsorbed on Graphene. *Nat. Mater.* **2007**, *6*, 652.
12. Wehling, T. O.; Novoselov, K. S.; Morozov, S. V.; Vdovin, E. E.; Katsnelson, M. I.; Geim, A. K.; Lichtenstein, A. I. Molecular Doping of Graphene. *Nano Lett.* **2008**, *8*, 173.
13. Echtermeyer, T. J.; Lemme, M. C.; Baus, M.; Szafranek, B. N.; Geim, A. K.; Kurz, H. Nonvolatile Switching in Graphene Field-effect Devices. *IEEE Electron Device Lett.* **2008**, *29*, 952.
14. Wang, X.; Li, X.; Zhang, L.; Yoon, Y.; Weber, P. K.; Wang, H.; Guo, J.; Dai, H. N-Doping of Graphene through Electrothermal Reactions with Ammonia. *Science* **2009**, *324*, 768–771.
15. Biel, B.; Triozon, F.; Blase, X.; Roche, S. Chemical Doping Effects on Charge Transport in Graphene Nanoribbons. *Nano Lett.* **2009**, *9*, 2725.
16. Loh, K. P.; Bao, Q.; Ang, P. K.; Yang, J. The Chemistry of Graphene. *J. Mater. Chem.* **2010**, 2277–2289.
17. Chen, J.-H.; Cullen, W. G.; Jang, C.; Fuhrer, M. S.; Williams, E. D. Defect Scattering in Graphene. *Phys. Rev. Lett.* **2009**, *102*, 236805.
18. Katsnelson, M. I.; Guinea, F.; Geim, A. K. Scattering of Electrons in Graphene by Clusters of Impurities. *Phys. Rev. B* **2009**, *79*, 195426.
19. Wehling, T. O.; Katsnelson, M. I.; Lichtenstein, A. I. Adsorbates on Graphene: Impurity States and Electron Scattering. *Chem. Phys. Lett.* **2009**, *476*, 125.
20. Boukhvalov, D. W.; Katsnelson, M. I. Chemical Functionalization of Graphene. *J. Am. Chem. Soc.* **2008**, *130*, 10697.
21. Boukhvalov, D. W.; Katsnelson, M. I. Chemical Functionalization of Graphene with Defects. *Nano Lett.* **2008**, *8*, 4373.
22. Robinson, J. P.; Schomerus, H.; Oroszlány, L.; Fal'ko, V. I. Adsorbate-Limited Conductivity of Graphene. *Phys. Rev. Lett.* **2008**, *101*, 196803.
23. Gómez-Navarro, C.; Weitz, R. T.; Bittner, A. M.; Scolari, M.; Mews, A.; Burghard, M.; Kern, K. Electronic Transport Properties of Individual Chemically Reduced Graphene Oxide Sheets. *Nano Lett.* **2007**, *7*, 3499.
24. Kaiser, A. B.; Gómez-Navarro, C.; Sundaram, R. S.; Burghard, M.; Kern, K. Electrical Conduction Mechanism in Chemically Derived Graphene Monolayers. *Nano Lett.* **2009**, *9*, 1787–1792.
25. Gómez-Navarro, C.; Meyer, J. C.; Sundaram, R. S.; Chuvilin, A.; Kurasch, S.; Burghard, M.; Kern, K.; Kaiser, U. *Nano Lett.* **2010**, *10*, 1144–1148.
26. Jung, I.; Dikin, D. A.; Piner, R. D.; Ruoff, R. S. Tunable Electrical Conductivity of Individual Graphene Oxide Sheets Reduced at Low Temperatures. *Nano Lett.* **2008**, *8*, 4283–4287.
27. Dreyer, D. R.; Park, S.; Bielawski, C. W.; Ruoff, R. S. The Chemistry of Graphene Oxide. *Chem. Soc. Rev.* **2010**, *39*, 228.
28. Elias, D. C.; Nair, R. R.; Mohiuddin, T. M. G.; Morozov, S. V.; Blake, P.; Halsall, M. P.; Ferrari, A. C.; Boukhvalov, D. W.; Katsnelson, M. I.; Geim, A. K.; Novoselov, K. S. Control of Graphene's Properties by Reversible Hydrogenation: Evidence for Graphane. *Science* **2009**, *323*, 610–613.
29. Chen, J. H.; Cullen, W. G.; Jang, C.; Fuhrer, M. S.; Williams, E. D. Defect Scattering in Graphene. *Phys. Rev. Lett.* **2009**, *102*, 236805.
30. Bostwick, A.; McChesney, J. L.; Emtsev, K. V.; Seyller, T.; Horn, K.; Kevan, S. D.; Rotenberg, E. Quasiparticle Transformation during a Metal-Insulator Transition in Graphene. *Phys. Rev. Lett.* **2009**, *103*, 056404.
31. Lee, G; Lee, B.; Kim, J.; Cho, K. Ozone Adsorption on Graphene: *Ab Initio* Study and Experimental Validation. *J. Phys. Chem. C* **2009**, *113*, 14225.
32. Mkhoyan, K. A.; Contryman, A. W.; Silcox, J.; Stewart, D. A.; Eda, G.; Mattevi, C.; Miller, S; Chhowalla, M. Atomic and Electronic Structure of Graphene Oxide. *Nano Lett.* **2009**, *9*, 1058.
33. Wehling, T. O.; Katsnelson, M. I.; Lichtenstein, A. I. Impurities on Graphene: Midgap States and Migration Barriers. *Phys. Rev. B* **2009**, *80*, 085428.
34. Barreiro, A.; Lazzeri, M.; Moser, J.; Mauri, F.; Bachtold, A. Transport Properties of Graphene in The High-Current Limit. *Phys. Rev. Lett.* **2009**, *103*, 076601.
35. Lherbier, A.; Blase, X.; Niquet, Y.-M.; Triozon, F.; Roche, S. Charge Transport in Chemically Doped 2D Graphene. *Phys. Rev. Lett.* **2008**, *101*, 036808.
36. Shon, N. H.; Ando, T. Quantum Transport in Two-Dimensional Graphite System. *J. Phys. Soc. Jpn.* **1998**, *67*, 2421.
37. Lee, P. A.; Ramakrishnan, T. V. Disordered Electronic Systems. *Rev. Mod. Phys.* **1985**, *57*, 287.
38. Moser, J.; Tao, H.; Roche, S.; Alsina, F.; Sotomayor Torres, C. M.; Bachtold, A. Magnetotransport in Disordered Graphene Exposed to Ozone: From Weak to Strong Localization. *Phys. Rev. B* **2010**, *81*, 205445.
39. Yan, J. A.; Xian, L.; Chou, M. Y. Structural and Electronic Properties of Oxidized Graphene. *Phys. Rev. Lett.* **2009**, *103*, 086802.
40. Ishii, H.; Roche, S.; Kobayashi, N.; Hirose, K. Inelastic Transport in Vibrating Disordered Carbon Nanotubes: Scattering Times and Temperature-Dependent Decoherence Effects. *Phys. Rev. Lett.* **2010**, *104*, 116801.
41. Yazyev, O. V. Emergence of Magnetism in Graphene Materials and Nanostructures. *Rep. Prog. Phys.* **2010**, *73*, 056501.
42. Soler, J. M.; Artacho, E.; Gale, J. D.; García, A.; Junquera, J.; Ordejón, P.; Sánchez-Portal, D. The Siesta Method for *Ab Initio* Order-N Materials Simulation. *J. Phys.: Condens. Mater.* **2002**, *14*, 2745.
43. Ceperley, D. M.; Alder, B. J. Ground State of the Electron Gas by a Stochastic Method. *Phys. Rev. Lett.* **1980**, *45*, 566.
44. Perdew, J. P.; Zunger, A. Self-Interaction Correction to Density-Functional Approximations for Many-Electron Systems. *Phys. Rev. B* **1981**, *23*, 5048.
45. Troullier, N.; Martins, J. L. Efficient Pseudopotentials for Plane-Wave Calculations. *Phys. Rev. B* **1991**, *43*, 1993.
46. Artacho, E.; Sánchez-Portal, D.; Ordejón, P.; García, A.; Soler, J. M. Linear-Scaling *Ab-Initio* Calculations for Large and Complex Systems. *Phys. Status Solidi B* **1999**, *215*, 809.
47. Roche, S.; Mayou, D. Conductivity of Quasiperiodic Systems: A Numerical Study. *Phys. Rev. Lett.* **1997**, *79*, 2518.
48. Roche, S. Quantum Transport by Means of O(N) Real-Space Methods. *Phys. Rev. B* **1999**, *59*, 2284.
49. Lherbier, A.; Biel, B.; Niquet, Y.-M.; Roche, S. Transport Length Scales in Disordered Graphene-based Materials: Strong Localization Regimes and Dimensionality Effects. *Phys. Rev. Lett.* **2008**, *100*, 036803.
50. Ishii, H.; Triozon, F.; Kobayashi, N.; Hirose, K.; Roche, S. Charge Transport in Carbon Nanotubes Based Materials: A Kubo-Greenwood Computational Approach. *C.R. Phys.* **2009**, *10*, 283–296.